Optical Properties of the Perovskite Solid Solution LaTiO2N-ATiO3 (A = Sr, Ba)

François Cheviré, Franck Tessier, Roger Marchand

Graphical abstract:

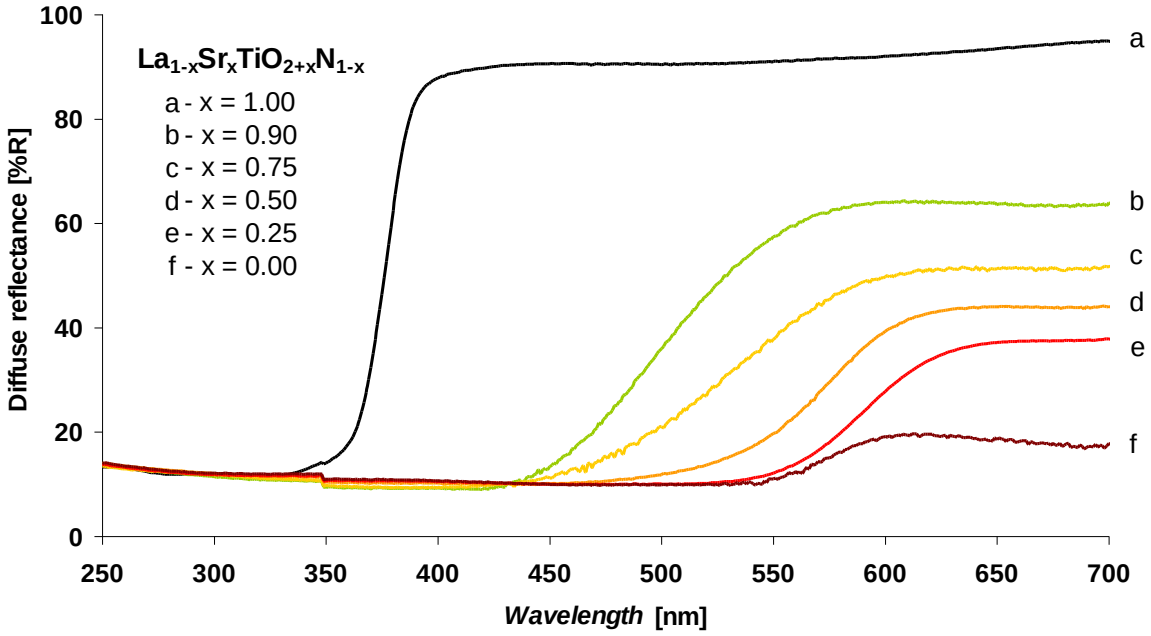

Optical properties of the perovskite solid solution $LaTiO_2N$-$ATiO_3$ (A = Sr, Ba).

François Cheviré, Franck Tessier *, Roger Marchand

UMR CNRS 6512 "Verres et Céramiques", Institut de Chimie de Rennes,
Université de Rennes 1,
F-35042 Rennes cedex, France
Phone: +33 2 23 23 62 56
Fax: +33 2 23 23 56 83
Franck.Tessier@univ-rennes1.fr

Keywords
Oxynitrides, perovskite, solid solution, optical properties

Abstract

Starting from the colored oxynitride $LaTiO_2N$, new perovskite-type solid solutions have been evidenced in the systems $La_{1-x}A_xTiO_{2+x}N_{1-x}$ (A = Sr, Ba) by ammonolysis at 950°C of corresponding oxide precursors prepared by molten salt route. The color of the resulting powders varies progressively from the brown of $LaTiO_2N$ to the white of the oxide with the decrease of both nitrogen and lanthanum contents. The optical absorption was characterized by diffuse reflectance. The non-linear variation of the optical bandgap may result from the competition between the variation of inductive effect between lanthanum and strontium, structure changes and the difference of electronegativity between nitrogen and oxygen. For the low nitrogen contents, the observed green shade is attributed to the presence of a nitrogen-rich secondary phase: TiO_xN_y in which titanium presents a mixed-valence state. Taking advantage of a chimie douce process, the amorphous citrate route, the highest oxidation state of titanium was stabilized until x = 0.9 in the $La_{0.1}Sr_{0.9}Ti(O,N)_3$ phase giving the powder a bright yellow color (Eg = 2.49 eV).

Introduction

The progressive insertion of nitrogen, a less electronegative element compared to oxygen, within an oxide network involves an increase in the covalent behavior of the bondings. From that substitution follows a lower optical gap value Eg, and consequently, a modification of the absorption properties of the compound. Although many oxides are white colored, corresponding oxynitrides are often colored. For example, considering the following cross-substitution: $M^{n+} + O^{2-} = M^{(n+1)+} + N^{3-}$, ZrO_2 (baddeleyite) and $BaTiO_3$ (perovskite) give rise respectively to isostructural colored oxynitrides TaON (yellow, Eg = 2,5 eV) and $BaTaO_2N$ (red brown, Eg = 2,0 eV). In the last few years, nitride-type materials have been largely studied for their optical potentialities as non-toxic colored pigments (see below), novel inorganic UV absorbers[1] or as visible light-driven photocatalysts.[2-5]

The first colored oxynitride perovskites were obtained by substituting titanium in $BaTiO_3$ by a V oxidation state element, such as tantalum or niobium. Numerous novel oxynitride phases were and are still obtained applying this substitution principle at both 12- and 6-fold coordinated cationic sites. This is a key principle at the origin of a rich chemistry. $ATaO_2N$ (A = Ca, Sr, Ba) and $ANbO_2N$ (A = Sr, Ba) manifest dielectric properties.[6,7] $BaTaO_2N$ and $BaNbO_2N$ crystallize in a cubic unit cell and $SrTaO_2N$ in a tetragonal one.[8-10] The substitution of barium by a lanthanide element results in oxynitrides $RTiO_2N$ (R = La, Nd)[11], where the IV oxidation state of titanium is stabilized due to the inductive effect of the rare earth element on the Ti-(O,N) bond.[12,13] This well-known effect is based on the capacity of an electropositive element (alkaline earth or rare earth) to share some electrons with the closest transition metal-nitrogen (oxygen) bond to enhance its covalent character, and thus to stabilize it. $NdTiO_2N$ is an orthorhombic $GdFeO_3$-type perovskite, while $LaTiO_2N$ crystallizes in a unit cell of triclinic symmetry.[14] The simultaneous substitution of both barium and titanium enables to have access to the white-colored phase $LaZrO_2N$, presenting also a deformed $GdFeO_3$-type perovskite structure[14], and otherwise to the oxynitride families $RTaON_2$ (R = La $\rightarrow$ Dy) and $LaNbON_2$.[11]

Based on one of the specific features of nitrogen: $\chi_N < \chi_O$, we attach a great interest working in oxynitride solid solution domains, as a suitable means to tune the optical properties with the progressive modification of the composition. Jansen et al. have shown the possibility to adjust the color of oxynitride pigments in the perovskite-type system $Ca_{1-x}La_xTaO_{2-x}N_{1+x}$.[15,16] In relation with the nitrogen content, the hue varies from yellow ($CaTaO_2N$) to brown ($LaTaON_2$) through orange and red intermediate colors. Grins et al. obtained similar results in the system $AZr_{1-x}Ta_xO_{3-x}N_x$ with powders evolving from the white of $AZrO_3$ to the yellow, red or brown of $ATaO_2N$, A

corresponding respectively to Ca, Sr and Ba.[17] Recently, Diot evidences solid solution domains in the perovskite systems A(A,Ta)(O,N,□)$_3$ (A= Ca, Sr, Ba) and Sr(Sr,Nb)(O,N,□)$_3$ giving rise to a range of colored pigments from pale yellow to orange brown.[18] Her research works have also shown the interest of defect fluorite rare earth tungstates - R_6WO_{12}□$_2$ and $R_{14}W_4O_{33}$□$_3$ (R = rare earth) - to isolate oxynitrides powders $R_6W(O,N,□)_{14}$ and $R_{14}W_4(O,N,□)_{36}$, the color of which changes progressively from the white of the oxides to bright yellow with increasing nitrogen substitution rate. While with large rare earth elements, the ammonolysis reaction of $RTaO_4$ tantalates provides either perovskite phases $RTaON_2$[11] or pyrochlore phases $R_2Ta_2O_5N_2$[19], Maillard et al. identified defect fluorite solid solutions $RTa(O,N,□)_4$ with small rare earths ($r_{R3+} \leq r_{Gd3+}$)[20]. Colored oxynitrides solid solution domains have been also obtained in other structure-types. Let us note, for example, orange compositions $Ta_{3-x}Zr_xN_{5-x}O_x$ ($0 \leq x \leq 0.60$) isostructural with Ta_3N_5 , and pale yellow $Ta_{1-x}Zr_xN_{1-x}O_{1+x}$ ($0 \leq x \leq 0.28$) isostructural with TaON[21].

This study was motivated, in part, by the preparation of light-colored oxynitride powders, for which an absorption edge exactly located at 400 nm will allow to absorb all UV radiations. Our objective was to evidence a solid solution domain $La_{1-x}A_xTiO_{2+x}N_{1-x}$ between the colored oxynitride $LaTiO_2N$ (brown, gap = 2.0 eV[22]) and the titanate $ATiO_3$ (A =Sr, Ba; gap > 3.1 eV) absorbing in the UV range.[1] $LaTiO_2N$ crystallizes in a distorted perovskite-type structure (Figure 1), as determined by neutron diffraction refinement, with a triclinic unit cell (I-1, a = 5.6097 Å, b = 7.8719 Å, c = 5.5772 Å, α = 90.199°, β = 90.154°, γ = 89,988°).[14] The structure reveals two distinct $Ti(O,N)_6$ octahedra and no nitrogen/oxygen ordering in the anionic network.

Results and Discussion

In a first step, we have considered the preparation of oxide precursors by molten salt synthesis. When x = 0, $La_2Ti_2O_7$ (layered perovskite structure) is clearly identified by X-ray diffraction. In the case of substituted compositions $La_{1-x}A_xTiO_y$, oxide precursors correspond generally to a mixture of ternary phases $La_aA_bTi_cO_d$ with variable composition. However, for x values close to 1, single phase powders present a perovskite structure close to that of the corresponding $ATiO_3$ titanate. Interestingly, the reaction under ammonia of these precursors leads systematically to the formation of single phase perovskite-type oxynitrides, even in the case of multinary oxides mixture (x < 1). Figure 2 illustrates particularly this observation with the example of the composition x = 0.5.

Table 1 details the experimental parameters of the performed ammonolysis experiments. All the compositions have a perovskite structure-type for which the position of the diffraction peaks

continuously shifts from $LaTiO_2N$ to $(Ba/Sr)TiO_3$, as observed for example in the case of strontium (Figure 3). Although the structure of $LaTiO_2N$ was refined in a triclinic unit cell using neutron diffraction, the diffraction lines of the corresponding X-ray diffraction pattern can be indexed in a cubic perovskite unit cell (a = 3.939(2) Å). The asymmetry of some peaks, previously reported [11], indicates that the real unit cell is not cubic. However, the distortion is quite weak, compared to that observed for $NdTiO_2N$, to determine unambiguously the unit cell by this technique. Here, it was not our purpose to refine all compositions of the solid solution by neutron diffraction. Using the cubic unit cell is an easy way to verify the linear evolution of the cell parameter and to prove the formation of the solid solution. Corresponding cubic unit cell parameters have been plotted versus x in Figure 4. The trend follows a linear relation, in both cases, in agreement with a Vegard's law. The opposite variation of the parameters, towards higher and lower values respectively for Ba- and Sr-substitution, is explained if we compare the cations size in 12-fold coordination (after Shannon[23] : La, 1.36 Å; Ba, 1.61 Å; Sr, 1.44 Å). There is a higher difference between La and Ba than for La and Sr, which should be balanced by the substitution of nitrogen by oxygen, with increasing x values. The resulting effect of such a competition within the lattices leads to the observed trend.

The brown color of the Ba-containing oxynitrides slightly lightens with increasing the alkaline earth metal amount from x = 0.3 to 0.5. But the composition with x = 0.75 presents a dark green shade we attribute to a partial reduction of titanium. A decrease of the reaction temperature to 900°C do not modify the green aspect of the color. In the case of Sr-containing oxynitrides, we observe a different color range strongly related to the substitution of a smaller size cation (Table 1). A study performed by Eng et al. [24] in the perovskite system $ATiO_3$ (A = Sr, Ca) attributes mainly to the distortion of the linear M-O-M bonds from Sr (180°) to Ca (156°) the formation of a narrow conduction band leading to a higher value of the band gap (+ 0.2 eV). This effect becomes more detectable with Ta compounds compared to those of Ti, due to the formation of larger conduction bands. This study just focus on the effects of the tilting of the octahedra and do not take in account neither inductive effect nor octahedra distorsions. With changing the alkaline earth metal, similar color and also band gap modifications have been observed in many phases, for example in the perovskite-type oxynitrides: $CaTaO_2N$ (yellow), $SrTaO_2N$ (orange red) and $BaTaO_2N$ (red brown). [7,8,10,25-27] In this series, the atomic ratio O/N is constant and only the effect of the earth-alkali can be distinguished from structure or inductive effect viewpoints. The characteristics of these phases are the following: $BaTaO_2N$ (cubic, band gap = 1.8 eV; Ta-(O,N)-Ta = 180°), $SrTaO_2N$ (tetragonal, band gap = 2.1 eV; Ta-(O,N)-Ta = 180° and 173.8°), $CaTaO_2N$ (orthorhombic, band gap = 2.4 eV; Ta-(O,N)-Ta = 153.9°). The linear evolution of the band gap from $BaTaO_2N$ to $CaTaO_2N$ do not parallel a linear change in the Ta-(O/N)-Ta angles. As $BaTaO_2N$ and $SrTaO_2N$ display similar bonding angles, we expect similar bandgaps for both of them, which is not the case. Thus, the

evolution of the band gap value, and also of the color, can not be only the consequence of the deviation from linearity of the M-O-M bonds. The color change is due to several parameters including structure changes and the influence of the weaker inductive effect of strontium compared to that of barium, leading to a less covalent compound.

According to reference [24], the band gap variation between $SrTiO_3$ (180°) and $CaTiO_3$ (156°) reaches 0.2 eV. However, in $LaTiO_2N$ (160-167°), the bonding angles range is closer to 180° compared to that in $CaTiO_3$, so that we can expect a lower influence on the band gap and a more diluted one for each of the intermediate compositions in the solid solution La-Sr-Ti-O-N. Between the two end members $LaTiO_2N$ and $SrTiO_3$, the only visible effect on the band gap position comes from the N/O substitution. The main consequence is an important red shift of the absorption edge. Thus, compared to the Ba-based system, for the same value of x, the absorption of the Sr-containing compositions is shifted towards lower wavelengths resulting in red and orange colored powders respectively for x = 0.25 and x = 0.50 instead of the brown powders observed for the Ba-containing compositions. In the present system, the color of the powders varies progressively from the brown of $LaTiO_2N$ to the white of the oxide $SrTiO_3$ with the decrease of the nitrogen content. However, the x = 0.9 composition is also characterized by a bright green shade close to the apple green color. This greenish color of the powder may be the consequence of a combination of a yellow hue with a black component. It is effectively known that a black-unsaturated yellow appears green, then khaki and finally black.

We ascribe the black shade to the presence of a mixed valent state titanium (Ti^{III}/Ti^{IV}). The origin of this phenomenon may be clarified according two hypotheses. First, the reduction of titanium may occur directly in the oxynitride product. It is then necessary to take account of a decrease of the formal cationic charge and consequently of a smaller nitrogen content in the structure as illustrated by the following formulations with x = 0.9:

$$(La_{1-x}Sr_x)Ti^{IV}O_{2+x}N_{1-x} \longrightarrow (La_{1-x}Sr_x)(Ti^{IV}_{1-y}Ti^{III}_{y})O_{2+(x+y)}N_{1-(x+y)}$$

$$(La_{0.1}Sr_{0.9})Ti^{IV}O_{2.9}N_{0.1} \longrightarrow (La_{0.1}Sr_{0.9})(Ti^{IV}_{1-y}Ti^{III}_{y})O_{2.9+y}N_{0.1-y}$$

Secondly, some reduced titanium may be present in a secondary black-colored phase, TiO_xN_y. The powder contains then a mixture of a nitrogen rich titanium oxynitride phase and a yellow-colored $La_{0.1}Sr_{0.9}Ti(O,N)_3$ oxynitride. However, no secondary phase was detected by XRD analyses (Figure 3). By experience, it is well known that a very small amount of impurity, even indiscernible by XRD, may be sufficient to alter completely the color of the product and to overestimate nitrogen titration results. In order to avoid any reduction of titanium, ammonolysis experiments were carried out at lower temperatures (until 850°C), but did not allow to stabilize the higher oxidation state of titanium since a green shade was still observable. Grins et al. report also similar color changes

within oxynitride solid solutions $AZr_xTa_{1-x}O_{2+x}N_{1-x}$ (A=Ca-Ba), without describing the hue progression.[16]

Nitrogen determination of the samples leads to the formulations listed in Table 2. Experimental contents are slightly higher than the calculated values (~ 2 %). In the case of the most greenish-colored composition (A = Ba and x = 0.75), the observed deviation (~ 4 %) is more important and seems to validate the hypothesis of a nitrogen rich secondary phase. In the strontium-based oxynitride series, the black component in the apple green shade is not very marked and supposes an extremely low amount of titanium oxynitride TiO_xN_y which does not affect considerably the measured nitrogen amount.

The optical characterization of $La_{1-x}Sr_xTi(O,N)_3$ oxynitrides by diffuse reflectance highlights several significant points (Figure 5). The plot of the corresponding spectra between the two end members of the solid solution confirms the shift of the absorption edge towards higher wavelengths with increasing nitrogen content. However, this shift is not progressive. Between the oxide $SrTiO_3$ and the oxynitride $La_{0.1}Sr_{0.9}Ti(O,N)_3$, the absorption edge moves from 375 to 500 nm - a shift of 125 nm - whereas it stays between 525 and 590 nm for the lanthanum-rich compositions. As an attempt to explain this non-linearity and despite of the difficulty to calculate the band structure due to nitrogen/oxygen disorder, it is realistic to involve the following effects. Basically, the element located in the 12-fold coordination site do not influence directly the bandgap, comprise between the 2p(O) and 3d(Ti) bands, but it rather engenders an inductive effect on the Ti-(O,N) bond. Besides the effect of the large cation, nitrogen/oxygen substitutions modify precisely the position of the valence band, so that the position of the absorption edge moves towards higher wavelengths. As nitrogen is less electronegative than oxygen, the energy level difference between oxygen and nitrogen 2p orbitals: $E_{2p}(O)$ = -14.8 eV, $E_{2p}(N)$ = -13.4 eV (top of the valence band[28]) can simply explain the decrease of the bandgap between valence and conduction bands. Also, as discussed above, by substituting La for Sr, the decrease of the bond angles from 180° causes a small increase of the band gap value that can act as a minor counter effect to the red shift (coupled with inductive effect variation) to explain parts of the non linearity of the band gap values along the solid solution. By comparison with the oxide $SrTiO_3$, the absorption edge profile appears less steep and the spectral selectivity lower (Table 3), as mainly a consequence of a lower crystallization state. We have already observed in oxide systems that the crystallization state of the powder influence the steepness of the diffuse reflectance spectrum. Thus, the absorption edge becomes steeper with increasing crystallization state. It is probably linked to the better homogeneity of the environments of titanium. The average octahedra is $TiO_{4+2x}N_{2-2x}$, but due to the O/N disorder we consent that a large variety of O/N environments with slightly different absorption properties should exist around

titanium atoms, leading to a spreading of the absorption edge. Moreover, the level of the reflexion plateau dramatically decreases with increasing nitrogen content. We have already observed, and not yet explained, such a phenomenon in several systems.[29,30] In the case of the composition x = 0.9, the absorption edge - located at 500 nm - should correspond to a yellow color although the powder appears "apple green" colored. This result brings another confirmation of the presence of a black component. Thus, the alteration of the expected color is effectively due to the existence of partially reduced titanium which is no more totally stabilized under the used reducing ammonia synthesis conditions.

In order to stabilize the IV oxidation state of titanium in the $La_{0.1}Sr_{0.9}Ti(O,N)_3$ oxynitride phase, a more reactive oxide precursor was synthesized by the amorphous citrate route. This chimie douce process allows to obtain rapidly very fine and chemically homogeneous powders, potentially able to manifest an enhanced reactivity with ammonia at lower temperature.[31,32] Experimental data are listed in Table 4 for both x = 0.9 and 1.0 compositions. A bright yellow powder is particularly obtained after ammonolysis of the x = 0.9 precursor at 950 °C. Reduction phenomenon did not occur with longer reaction time. The corresponding diffuse reflectance spectra, shown on Figure 6, reveals an absorption domain at the same wavelengths than for the absorption of the greenish product obtained from the molten salt precursor. Moreover, a slight gain is noticed in the maximum of diffuse reflectance, in possible relation with the disappearance of the black component discussed previously. In addition, the experimental nitrogen content of this phase reaches 0.8_1 wt%, in excellent agreement with the calculated content (0.74 wt%), and corresponds to the following formulation $La_{0.10}Sr_{0.90}TiO_{2.89}N_{0.11}$. All those results confirm the hypothesis of the presence of a small amount of titanium oxynitride as an impurity in the former results since the use of a more chemically homogeneous precursors solve the problem. Nevertheless, the green shade appears again for the composition x = 0.05, the powder becoming green yellowish. In this case, we are in the presence of a very small amount of dopant and it is difficult to conclude about the origin of the reduced titanium giving the green shade and the nature of the "impurity" phase. Many possibilities are of interest as the presence of a TiO_xN_y or $SrTi(O,N,\square)_3$ secondary phase. A reaction under ammonia at 750°C produces a pale green powder without any marked yellow hue. It seems that under usual ammonolysis conditions the reduction of titanium occurs before the maximum nitrogen content is obtained.

To conclude, we have synthesized new oxynitride solid solutions in the systems $La_{1-x}A_xTiO_{2+x}N_{1-x}$ (A = Sr, Ba), where it is possible to tune progressively the color of the powders progressively from brown ($LaTiO_2N$), to red, orange, yellow and finally white ($SrTiO_3$) with the variation of both nitrogen and lanthanum contents. The green shade observed in the presence of low nitrogen contents is attributed to mixed valent titanium present in a black nitrogen-rich phase:

TiO_xN_y. An attenuation of this reduction phenomenon is detected when using more chemically homogeneous and reactive precursors prepared by the amorphous citrate route. Such processes bring a suitable solution to optimize the properties of (oxy)nitride materials for optical applications (colored pigments, visible-light photocatalysts…). Avoiding such parasitic color is a major synthetic problem to solve in the preparation of light colored materials for promising applications as novel UV absorbers. Nevertheless, the interest of oxynitride solid solution domain relies here on the possibility to tune the absorption edge position towards 400 nm, limit between the UV and the visible ranges.

Experimental

Oxide precursors synthesis. Lanthanum-modified titanates were obtained using both a modified ceramic route and by taking advantage of the amorphous citrate route - a *chimie douce* method - which gives the oxide precursors an enhanced homogeneity and reactivity towards ammonia.

Solid state route. $La_{1-x}A_xTiO_{3.5-x/2}$ precursors (x = 0, 0.25, 0.5, 0.75, 0.9) were prepared by heating a stoichiometric mixture of La_2O_3 (99.99%, Alfa Aesar), $BaCO_3$ (99%, Acros), $SrCO_3$ (99%, Alfa Aesar) and TiO_2 (Degusa, P25) in a molten salt medium. The melt content, corresponding to the eutectic mixture 50 mol. % NaCl - 50 mol. % KCl, is determined to form 50 wt. % of the total reactants weight.[33] The corresponding mixture was heated at 1000 °C during 15 h in a muffle furnace. The resulting products were washed using distilled water and absolute ethyl alcohol, then dried at 150 °C.

*Amorphous citrate route***.** Among numerous *chimie douce*-type processes which have been developed to prepare oxide powders in order to improve their quality (purity, chemical homogeneity, etc.) and their reactivity, the process involving citric acid as a complexing agent was preferentially used. It is not, strictly speaking, a classic sol-gel process in the usual sense that the gel is not formed by a metal-oxygen-metal network, but rather from calcination of metal-organic complexes, thus producing ultrafine reactive powders with an excellent chemical homogeneity.[34] In order to characterize any influence of the synthesis route, the x = 0.9 precursor for A = Sr was also prepared using this route. Lanthanum oxide (La_2O_3, 99.99%, Alfa Aesar), strontium carbonate ($SrCO_3$, 99%, Alfa Aesar) and titanium tetrabutoxide ($C_{16}H_{36}O_4Ti$, 99%, Acros) were used as starting materials and dissolved in a diluted nitric acid solution. Citric acid ($C_6H_8O_7$, Merck, > 99%) dissolved in a minimum amount of water was added to the solution in the proportion of one mole per cation valence, the addition being followed by a 30 min stirring step at 120 °C. As the complexation of cations by citric acid is improved at pH ≥ 7, the acidic solution was neutralized by an ammonia solution (25 %, Merck)[35], then stirred at 150 °C for 15 min to promote chelate

formation. The liquid was progressively heated up to 250 °C, leading after 15 h to an expanded black solid residue. This solid was finally ground and calcined at 600 °C in an alumina crucible until total elimination of carbon.

Thermal ammonolysis. Nitridation reactions were carried out in alumina boats placed inside an electric furnace through which ammonia gas flowed at 40-50 L h^{-1}. The temperature was raised to the 950-1000 °C range with a heating rate of 10 °C min^{-1}. After a reaction time of 15 h, the furnace was switched off and the nitrided powders were allowed to cool to room temperature under a pure nitrogen atmosphere.

X-ray diffraction. XRD powder patterns were recorded using a Philips PW3710 diffractometer operating with Cu K_α radiation (λ = 1.5418 Å). X'PERT softwares-Data Collector and Graphics and Identify-were used, respectively, for recording, analysis, and phase matching of the patterns. The lattice parameters were refined using Dicvol04.[36]

Elemental analysis. Nitrogen and oxygen contents were determined with a LECO TC-436 analyzer using the inert gas fusion method. Nitrogen was detected as N_2 by thermal conductivity and oxygen as CO_2 by infrared detection. The apparatus was calibrated using N_2 and CO_2 gas (purity ≥ 99.95%) as well as ε-TaN as a nitrogen standard.[37]

UV-Vis spectrophotometry. Diffuse reflectance spectra were collected using a Varian Cary 100 Scan spectrometer equipped with the Varian WinUV software and the integrating sphere Labsphere (DRC-CA-30I). Prior to measurements, the absolute reflectance of the samples was calibrated with a certified "spectralon" standard (Labsphere Cie). Experimental data were collected within the 250-800 nm range with 1 nm step and 0.5 s integration time. The position of the absorption edge was determined graphically at the inflexion point of the curve and the value of the optical gap using the theory of Kubelka-Munk.[38]

References

[1] F. Cheviré, Thesis n° 3061, Université de Rennes 1, France, **2004**.

[2] D. Li, H. Haneda, S. Hishita, N. Ohashi, *Mater. Sci. Eng. B* **2005**, *117*, 67-75.

[3] D. Yamasita, T. Takata, M. Hara, J. N. Kondo, K. Domen, *Solid State Ionics* **2004**, *172*, 591-595.

[4] M. Hara, T. Takata, J. N. Kondo, K. Domen, *Catal. Today* **2004**, *90*, 313-317.

[5] A. Kasahara, K. Nukumizu, T. Takata, J. N. Kondo; M. Hara, H. Kobayashi, K. Domen, *J. Phys. Chem. B* **2003**, *107*, 791-797.

[6] R. Marchand, F. Pors, Y. Laurent, *Rev. Int. Tempér. Réfract. Fr.* **1986**, *23*, 11-15.

[7] F. Pors, R. Marchand, Y. Laurent, P. Bacher, G. Roult, *Mater. Res. Bull.* **1988**, *23***,** 11-15.

[8] F. Pors, P. Bacher, R. Marchand, Y. Laurent, G. Roult, *Mater. Res. Bull.* **1988**, *23***,** 1447-1450.

[9] F. Pors, P. Bacher, R. Marchand, Y. Laurent, G. Roult, *Rev. Int. Tempér. Réfract. Fr.* **1988**, *24***,** 239-246.

[10] Y.-I. Kim, P. M. Woodward, K. Z. Baba-Kishi, C. W. Tai, *Chem. Mater.* **2004**, *16*, 1267-1276.

[11] R. Marchand, F. Pors, Y. Laurent, *Ann. Chim. Fr.* **1991**, *16*, 553-560.

[12] J. Etourneau, J. Portier, F. Ménil, *J. Alloys Comp.* **1992**, *188*, 1-7.

[13] H. -C. Zur Loye, J. D. Houmes, D. S. Bem, *The chemistry of Transition Metal Carbides and Nitrides*, Ted Oyama Ed., Blackie Academic & Professional, **1996**, *8*, 155.

[14] S. J. Clarke, B. P. Guinot, C. W. Michie, M. J. C. Calmont, M. J. Rosseinsky, *Chem. Mater.* **2002**, *14*, 288-294.

[15] M. Jansen, H. P. Letschert, *Nature* **2000**, *404*, 980-982.

[16] M. Jansen, H. P. Letschert, *European Patent n° 0627373,* **1995**.

[17] J. Grins, G. Svensson, *Mater. Res. Bull.* **1994**, *29*, 801-809.

[18] N. Diot, Thesis n° 2222, Université de Rennes 1, France, **1999**.

[19] F. Pors, R. Marchand, Y. Laurent, *J. Solid State Chem.* **1993**, *107*, 39-42.

[20] P. Maillard, F. Tessier, E. Orhan, F. Cheviré, R. Marchand, *Chem. Mater.* **2005**, *17*, 152-156.

[21] E. Günther, M. Jansen, *Mater. Res. Bull.* **2001**, *36*, 1399-1405.

[22] G. Hitoki, T. Takata, J. N. Kondo, M. Hara, H. Kobayashi, K. Domen, *Electrochem.* **2002**, *70*, 463-465.

[23] R. D. Shannon, *Acta Cryst.* **1976**, *A32*, 751-767.

[24] H. W. Eng, P. W. Barnes, B. M. Auer, P. M. Woodward, *J. Solid State Chem.* **2003**, *175*, 94-109.

[25] F. Pors, P. Bacher, R. Marchand, Y. Laurent, G. Roult, *Rev. Int. Hautes Tempér. Réfract.* **1987**, *24*, 239-246.

[26] E. Günther, R. Hagenmayer, M. Jansen, *Z. Anorg. Allg. Chem.* **2000**, *626*, 1519-1525.

[27] S. J. Clarke, K. A. Hardstone, C. W. Michie, M. J. Rosseinsky, *Chem. Mater.* **2002**, *14*, 2664-2669.

[28] R. Hoffmann, *J. Chem. Phys.* **1963**, *39*, 1397-1412.

[29] F. Cheviré, F. Tessier, R. Marchand, *Sil. Ind.* **2004**, *69*, 159-163.

[30] N. Diot, O. Larcher, R. Marchand, J.Y. Kempf, P. Macaudière, *J. Alloys Comp.* **2001**, *323-324*, 45-48.

[31] F. Cheviré, F. Tessier, R. Marchand, *Mater. Res. Bull.* **2004**, *39*, 1091-1101.

[32] P. Maillard, F. Tessier, E. Orhan, F. Cheviré, R. Marchand, *Chem. Mater.* **2005**, *17*, 152-156.

[33] P.A. Fuierer, R.E. Newnham, *J. Am. Ceram. Soc.* **1991**, *74*, 2876-2881.

[34] F. Tessier, R. Marchand, *J. Solid State Chem.* **2003**, *171*, 143-151.

[35] A. Douy, P. Odier, *Mater. Res. Bull.* **1989**, *24*, 1119-1126.

[36] A. Boultif, D. Louer, *J. Appl. Cryst.* **2004**, *37*, 724-731.

[37] M. Dopita, B. Wollein, D. Rafaja, W. Gruner, W. Lengauer, *Defect and Diffusion Forum, Diffusion in Materials* DIMAT-2000 **2001**, *194-199*, 1607-1612.

[38] D. Kubelka, L. Munk, *Z. Teck. Physik.* **1931**, *12*, 593-601.

Figures and tables captions

Figure 1: Crystal structure of the oxynitride perovskite $LaTiO_2N$.

Figure 2: XRD powder pattern of the $La_{0.5}Ba_{0.5}TiO_{2.48}N_{0.52}$ oxynitride after ammonolysis of the corresponding oxide precursor.

Figure 3: XRD patterns of the $La_{1-x}Sr_xTi(O,N)_3$ compositions (prepared at 950°C) between the end terms of the solid solution.

Figure 4: Variation of the unit cell parameter in the $La_{1-x}Ba(Sr)_xTi(O,N)_3$ solid solutions.

Figure 5: Diffuse reflectance spectra of $La_{1-x}Sr_xTi(O,N)_3$ compositions.

Figure 6: Comparison of the diffuse reflectance spectra of $La_{0.10}Sr_{0.90}TiO_{2.89}N_{0.11}$ prepared by ammonolysis of the molten salt and citrate precursors.

Table 1: Experimental parameters for $La_{1-x}A_xTi(O,N)_3$ (A = Sr, Ba) oxynitrides.

Table 2: Nitrogen contents and corresponding oxynitride formulations.

Table 3: Diffuse reflectance data of the oxynitride $La_{1-x}Sr_xTi(O,N)_3$ series obtained from precursors prepared by molten salt synthesis.

Table 4: Experimental data of the synthesis of $La_{0.1}Sr_{0.9}Ti(O,N)_3$ oxynitrides using the citrate route.

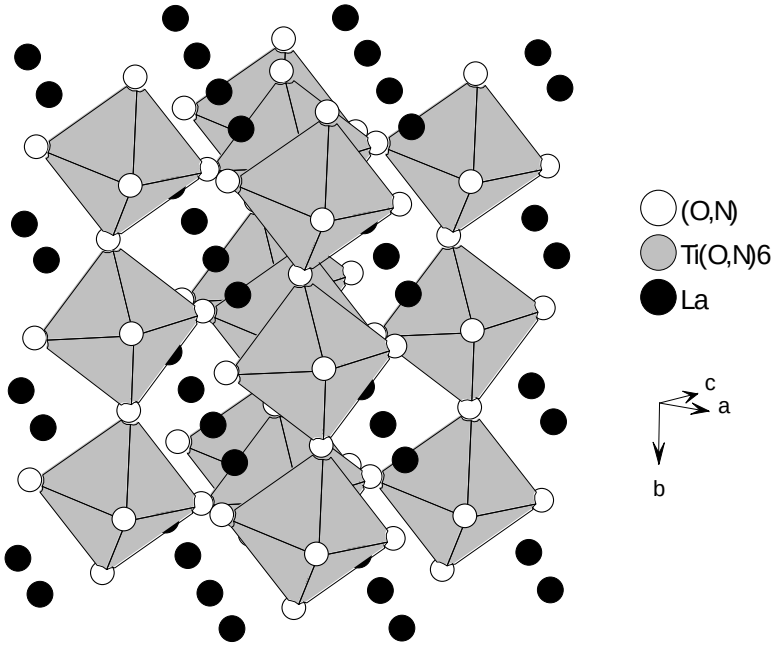

Figure 1

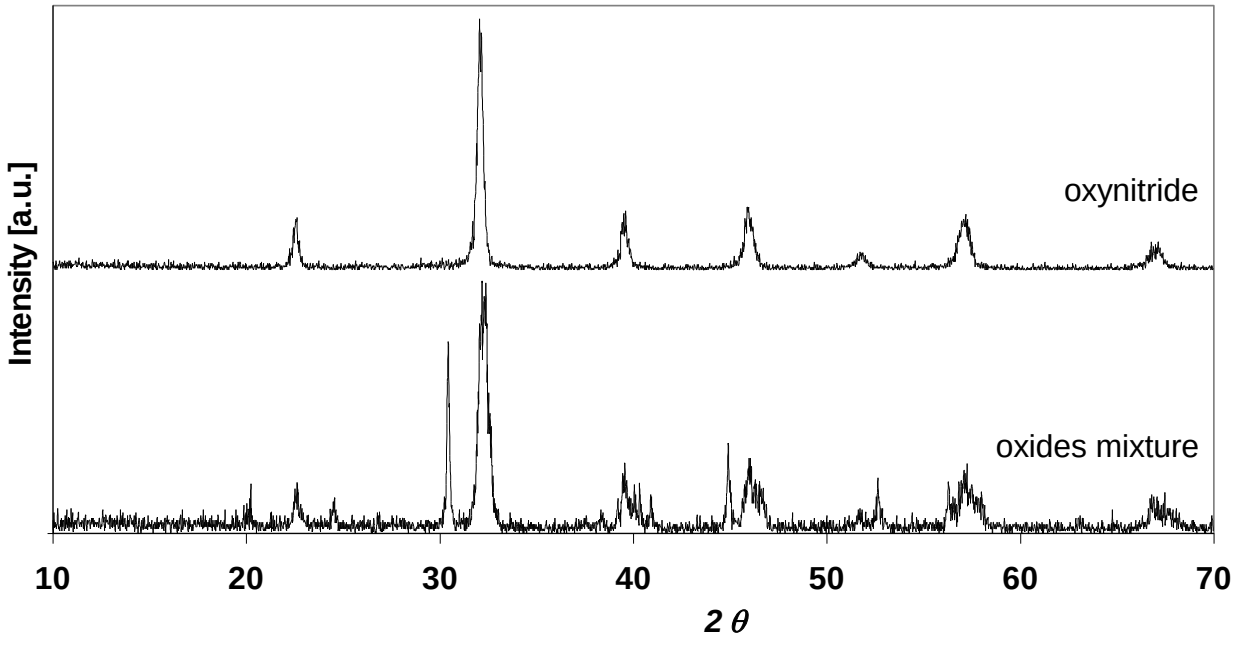

Figure 2

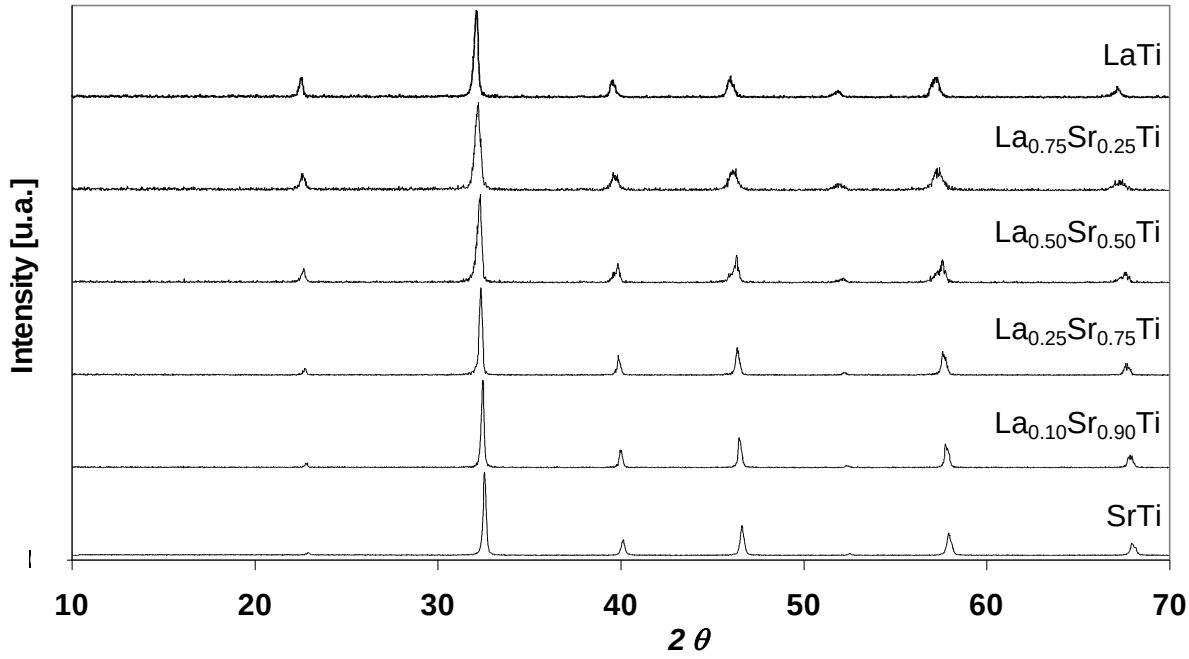

Figure 3

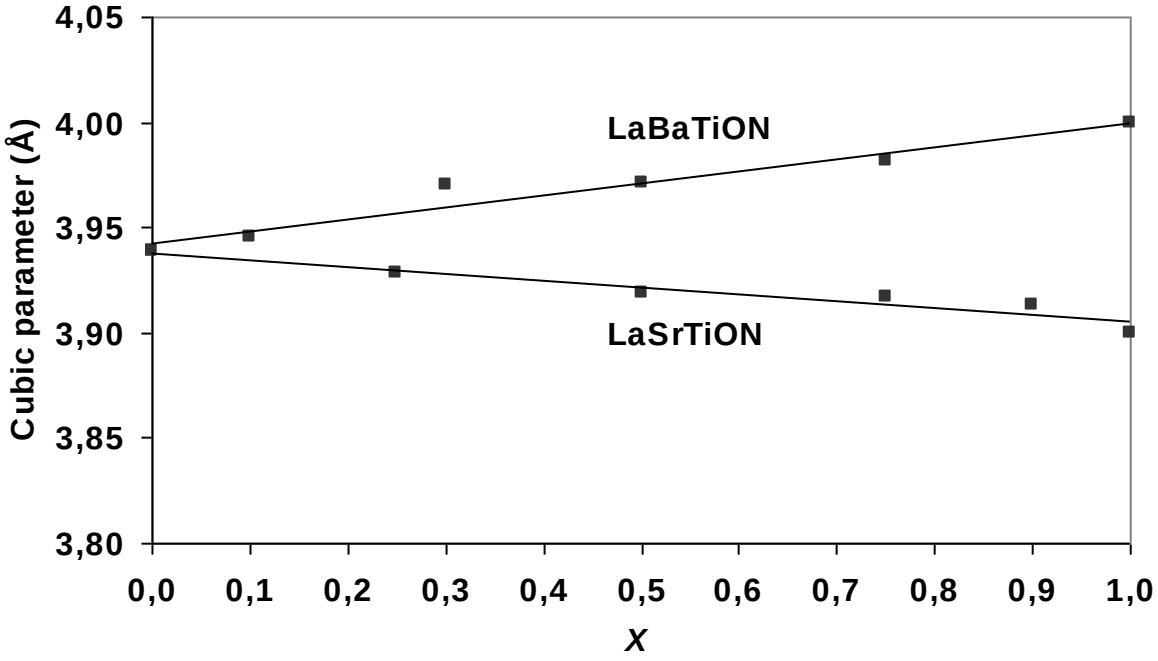

Figure 4

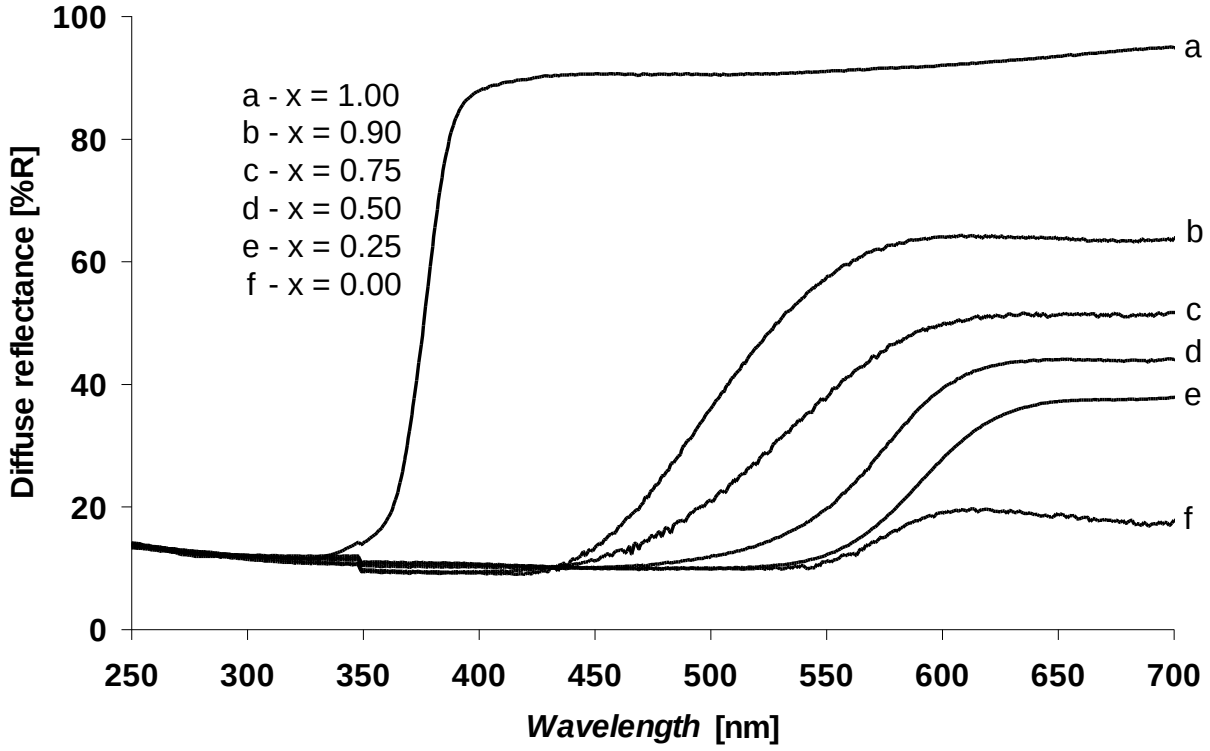

Figure 5

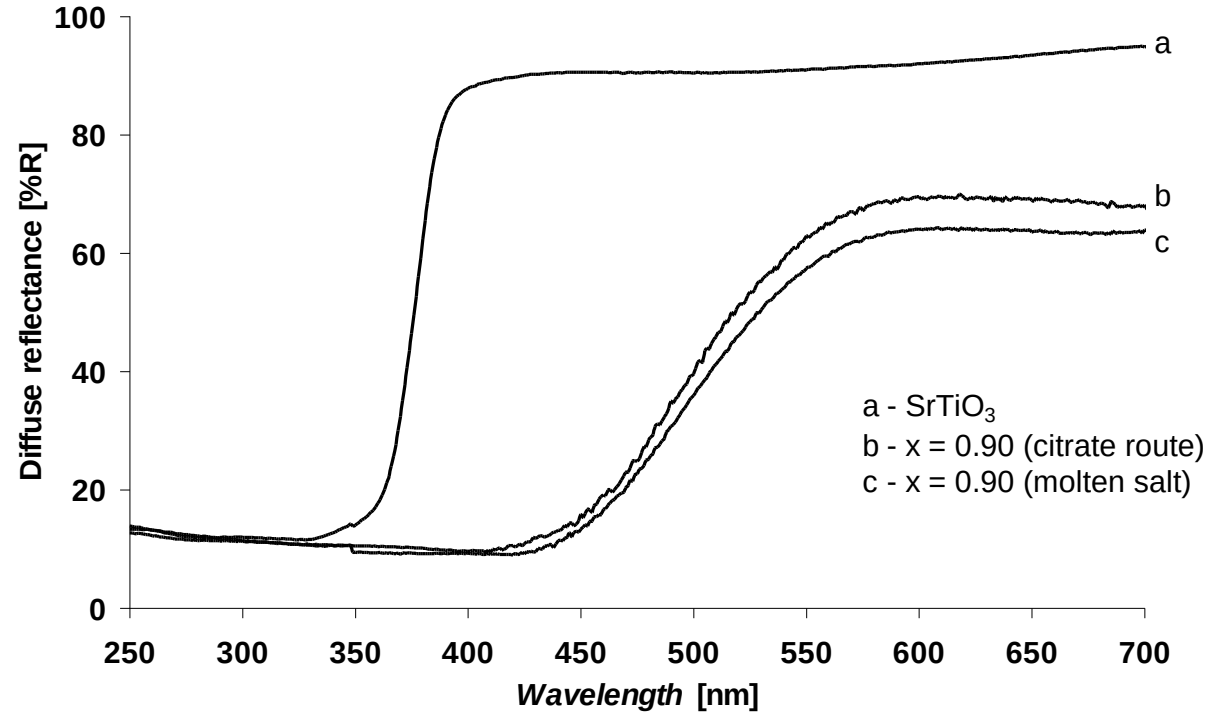

Figure 6

Table 1

Cationic composition	Nitridation parameters	Cubic unit cell parameter* (Å)	Powder color
LaTi	950°C/NH_3/15h	3.939(2)	brown
$La_{0.90}Ba_{0.10}Ti$	950°C/NH_3/15h	3.945(2)	brown
$La_{0.70}Ba_{0.30}Ti$	950°C/NH_3/15h	3.970(3)	brown
$La_{0.50}Ba_{0.50}Ti$	950°C/NH_3/15h	3.971(2)	pale brown
$La_{0.25}Ba_{0.75}Ti$	900°C/NH_3/15h	-	khaki
$La_{0.25}Ba_{0.75}Ti$	950°C/NH_3/15h	3.982(1)	dark green
$La_{0.75}Sr_{0.25}Ti$	950°C/NH_3/15h	3.928(2)	red
$La_{0.50}Sr_{0.50}Ti$	950°C/NH_3/15h	3.9187(4)	orange
$La_{0.25}Sr_{0.75}Ti$	950°C/NH_3/15h	3.917(1)	ocher
$La_{0.10}Sr_{0.90}Ti$	850°C/NH_3/15h	-	green
$La_{0.10}Sr_{0.90}Ti$	950°C/NH_3/15h	3.9130(3)	apple green

* refined values (using Dicvol04[36])

Table 2

Cationic composition	N wt. % $_{calc.}$	N wt. % $_{exp.}$	Experimental formulation
LaTi	6.02	6.1_7	$LaTiO_{1.96}N_{1.02}$
$La_{0.90}Ba_{0.10}Ti$	5.41	5.5_5	$La_{0.90}Ba_{0.10}TiO_{2.07}N_{0.92}$
$La_{0.70}Ba_{0.30}Ti$	4.21	4.4_3	$La_{0.70}Ba_{0.30}TiO_{2.27}N_{0.73}$
$La_{0.50}Ba_{0.50}Ti$	3.01	3.1_4	$La_{0.50}Ba_{0.50}TiO_{2.48}N_{0.52}$
$La_{0.25}Ba_{0.75}Ti$	1.50	2.0_5	$La_{0.25}Ba_{0.75}TiO_{2.62}N_{0.34}$
$La_{0.75}Sr_{0.25}Ti$	4.77	4.9_1	$La_{0.75}Sr_{0.25}TiO_{2.22}N_{0.77}$
$La_{0.50}Sr_{0.50}Ti$	3.36	3.5_2	$La_{0.50}Sr_{0.50}TiO_{2.47}N_{0.52}$
$La_{0.25}Sr_{0.75}Ti$	1.79	2.0_6	$La_{0.25}Sr_{0.75}TiO_{2.69}N_{0.29}$
$La_{0.10}Sr_{0.90}Ti$	0.74	0.9_1	$La_{0.10}Sr_{0.90}TiO_{2.88}N_{0.12}$

Table 3

Composition	$\lambda \pm \Delta\lambda$ (nm)	Eg (eV)
$SrTiO_3$	376 ± 14	3.31
$La_{0.10}Sr_{0.90}Ti(O,N)_3$	497 ± 63	2.49
$La_{0.25}Sr_{0.75}Ti(O,N)_3$	533 ± 60	2.27
$La_{0.50}Sr_{0.50}Ti(O,N)_3$	574 ± 38	2.07
$La_{0.75}Sr_{0.25}Ti(O,N)_3$	590 ± 33	2.02
$LaTiO_2N$	574 ± 30	1.96

Table 4

Cationic composition	Experimental parameters	Color	$\lambda \pm \Delta\lambda$ (nm)
SrTi	950°C/air/15h	white	376 ± 20
$La_{0.10}Sr_{0.90}Ti$	950°C/NH_3/15h	bright yellow	-
$La_{0.10}Sr_{0.90}Ti$	950°C/NH_3/2x15h	bright yellow	496 ± 57
$La_{0.05}Sr_{0.95}Ti$	750°C/NH_3/15h	pale green	-
$La_{0.05}Sr_{0.95}Ti$	900°C/NH_3/2x15h	pale yellow / green	483 ± 55
$La_{0.05}Sr_{0.95}Ti$	950°C/NH_3/15h	green	-